Inorganic Chemistry

ARTICLE

pubs.acs.org/IC

Redox Trends in Terpyridine Nickel Complexes

James T. Ciszewski,[†] Dmitry Y. Mikhaylov,[‡] Kirill V. Holin,[‡] Marsil K. Kadirov,[‡] Yulia H. Budnikova,[*,‡] Oleg Sinyashin,[‡] and David A. Vicic[*,†]

[†]Department of Chemistry, University of Hawaii, 2545 McCarthy Mall, Honolulu, Hawaii 96822, United States

[‡]A.E. Arbuzov Institute of Organic and Physical Chemistry, Kazan Scientific Center of Russian Academy of Sciences, 8, Arbuzov Str., 420088 Kazan, Russian Federation

S *Supporting Information*

ABSTRACT: A synthesis has been developed that allows the isolation of four-coordinate [(tpy)Ni-Br] (**1**, tpy = terpyridine) in high yield. Complex **1** has been structurally characterized, and the X-ray data reveal a square-planar geometry, unlike the known [(tpy′)Ni-I] (tpy′ = 4,4′,4″-tri-*tert*-butyl-terpyridine) but similar to [(tpy)Ni-CH_3]. In the solid-state, EPR spectroscopy indicates, however, that unlike [(tpy)Ni-CH_3], the electronic structure of **1** is a metal-centered, not a ligand-centered radical. Density functional theory (DFT) analyses support this assignment. The preparation of **1** also facilitated the analysis of the redox potentials of a series of terpyridine nickel derivatives. It was found that the overall ligand sphere (one vs two coordinated terpyridine ligands) plays more of a role in determining the redox potentials of these derivatives than do the formal oxidation states of the nickel ions in the solution phase.

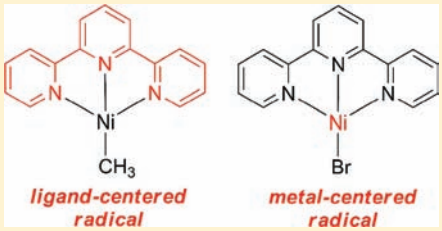

INTRODUCTION

Four-coordinate terpyridine nickel halide complexes are believed to be involved in a number of important organic transformations recently developed. It was first reported in 2004 that terpyridine nickel complexes can catalyze the cross-coupling of alkyl halides with alkyl nucleophiles (eq 1) via putative [(tpy)-Ni-X] intermediates.[1] Further mechanistic work, both experimental[2,3] and computational,[4] supported the involvement of these four-coordinate nickel halide intermediates in the cross-couplings. Terpyridyl nickel halides are also expected to be involved in the room-temperature Negishi approaches to C-alkyl and C-aryl glycosides developed by Gagné (eq 2).[5,6] Moreover, Gagné also found that the same terpyridine salts of nickel can catalyze the reductive coupling of glycosyl bromides with activated alkenes (eq 3).[7] Budnikova provided direct evidence of the importance of four-coordinate [(tpy)NiBr] by showing that electrochemical reduction of [(tpy)$NiBr_2$] by one electron leads to an active species that can catalyze the addition of perfluoroalkyl radicals to olefins, eq 4.[8,9] Weix found that, under the right conditions, the coupling reactions involving nickel terpyridine complexes could be tuned to form high yields of reductive dimerization products (eq 5).[10] Most recently, Bisco found that secondary alkylzinc halides can be coupled to aryl iodides with excellent isomeric retentions using a nickel terpyridine system (eq 6).[11] Despite the above successes involving [(tpy)Ni-X], little is known about the fundamental physical properties of these species. Herein we report a convenient synthesis of [(tpy)Ni-Br] (1) along with the structural, magnetic, and electrochemical studies that the synthesis has enabled.

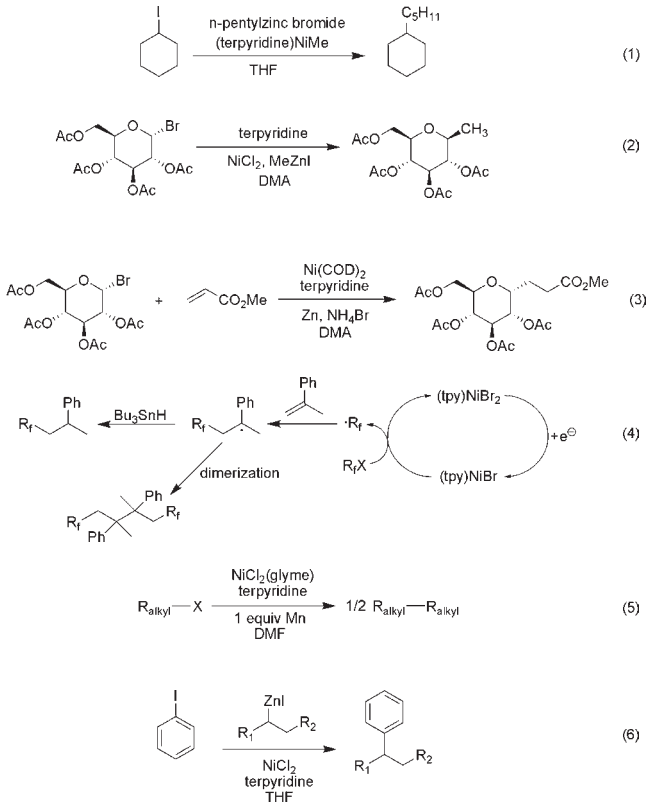

Received: June 1, 2011
Published: July 28, 2011

 © 2011 American Chemical Society

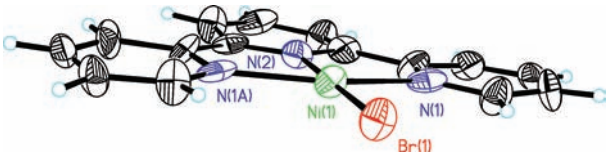

Figure 1. ORTEP diagram of **3**. Ellipsoids shown at 50%. Selected bond lengths (Å): Ni−Br 2.447(11); Ni−N1 2.094(16); Ni−N2 2.04(2). Selected bond angles (deg): N2−Ni−Br 180.000(2); N2−Ni−N1 79.2(4), N1−Ni−Br 100.8(4), N1−Ni−N1a 158.5(8).

Chart 1. Representations of 1 with Different Electronic Structures, Depending on Whether the Unpaired Electron Resides Primarily on the Metal (Left) or on the Ligand (Right)

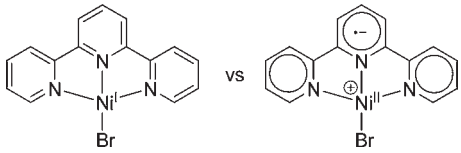

RESULTS AND DISCUSSION

Preparation of [(tpy)Ni-I] is known to proceed by the reaction of [(tpy)Ni(COD)] with 1 equiv of methyl iodide.[1] The preparation of the [(tpy)Ni-Br] congener, however, is more complicated as the terpyridine nickel(0) species is known to be less active toward alkyl bromides. Therefore, alternative routes to prepare **1** were explored. The best route was found to involve the comproportionation reaction of [(dme)$NiBr_2$] and $Ni(COD)_2$ in the presence of 2 equiv of terpyridine as described in eq 7. This reaction was driven to high yields of product formation (72% isolated) by the precipitation of **1** from THF solvent. Complex **1** is a dark green air-sensitive compound which is insoluble in most organic solvents. Crystals can be grown from dimethylformamide (DMF) solutions layered with toluene, and the ORTEP diagram of **1** is shown in Figure 1.

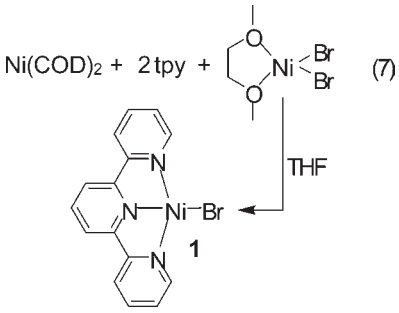

Compound **1** crystallizes in the $C2/c$ space group with one-half of the molecule related by symmetry. Full analysis of the X-ray data show that molecules of **1** pack in sheets with head-to-tail arrangements of the flat molecules as shown in Figure 2. We speculate that these efficient packing arrangements contribute to the overall insolubility of the complex. The most unique feature of the structure of complex **1** is that surprisingly, unlike [(tpy′)NiI],[1] **1** crystallizes in a square-planar geometry. With this geometry in mind, the location of the unpaired electron (Chart 1) becomes an issue as the vast majority of square-planar nickel complexes consist of nickel in the plus two oxidation state. Since the related compound [(tpy)Ni-CH_3] (**2**) also crystallizes in a square-planar arrangement with an electronic structure that is most appropriately described as [$(tpy^{-1})Ni^{II}-CH_3$],[2] it is tempting to say that the most proper way to describe **1** is the similar form shown to the right of Chart 1. However, the electron paramagnetic resonance (EPR) spectroscopy and density functional theory (DFT) studies provided in this paper suggest that analogies between [(tpy)Ni-CH_3] and **1** based solely on X-ray crystallographic evidence may not be appropriate.

The low-temperature solid-state powder EPR spectrum of **1** (Figure 3) exhibits an axial signal with $g_{\parallel} = 2.256$ and $g_{\perp} = 2.091$ consistent with a metal-centered $d_{x^2-y^2}$ ground state. In DMF solution, an isotropic signal can be observed with $g_{iso} = 2.139$. Thus, both in the crystal structure form and in solution, signals for a radical with substantial metal character are observed for **1**. These EPR results are telling in that the electronic structure of **1** is significantly different than that of [(tpy)Ni-CH_3] (**2**) as the g-values of **2** were more indicative of a ligand-centered radical ($g_{iso} = 2.021$ at room temperature and $g_x = 2.056$, $g_y = 2.021$, and $g_z = 1.999$ at 77 K).[2]

The cyclic voltammogram for **1** is shown in Figure 4, and reveals that two quasi-reversible reductions occur at −0.76 V and −1.35 vs Ag/AgCl in DMF solvent. Intriguingly, we found that reductions of the related dibromide [(tpy)$NiBr_2$] occur at the same potentials (see below). To probe the solution redox chemistry further, titrations were performed to provide a full analysis of different species containing the terpyridine ligand. Figure 5 shows the evolution of the cyclic voltammograms when the synthesis conditions outlined in eq 7 are repeated in DMF solvent containing various amounts of [(DME)$NiBr_2$]. Initially, only [$Ni(COD)_2$] plus 2 equiv of terpyridine are present in solution (Figure 5, black line). Two reversible waves are seen at −1.12 and −1.42 V vs Ag/Ag^+, and since the nickel is formally in the zero oxidation state, these waves correspond to two ligand-

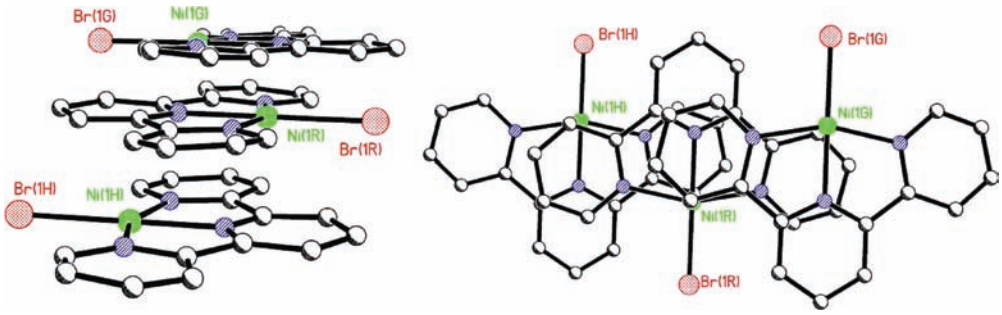

Figure 2. Partial representations of the packing diagram for crystallized **1**. The shortest intermolecular contact (distance between the nickel and carbon atoms of the ligand) is 3.239 Å.

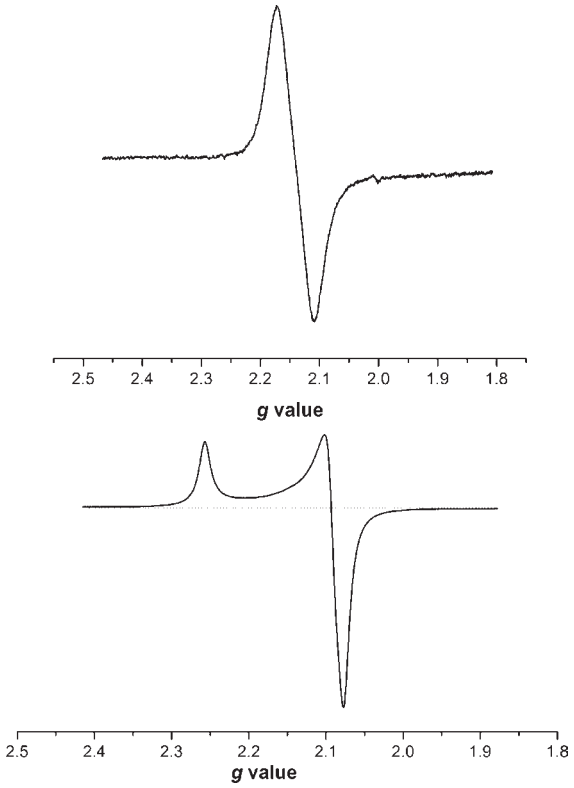

Figure 3. Top: Room temperature EPR spectrum of **1** in DMF solvent at 296 K. Parameters: microwave frequency 9.461749 GHz; microwave power 6.325 mW; modulation amplitude 10 G; receiver gain 31697.86. Bottom: Powder EPR spectrum of **1** at 200 K. Parameters: microwave frequency 9.448628 GHz; microwave power 0.4 mW; modulation amplitude 0.10 G; receiver gain 5023.773.

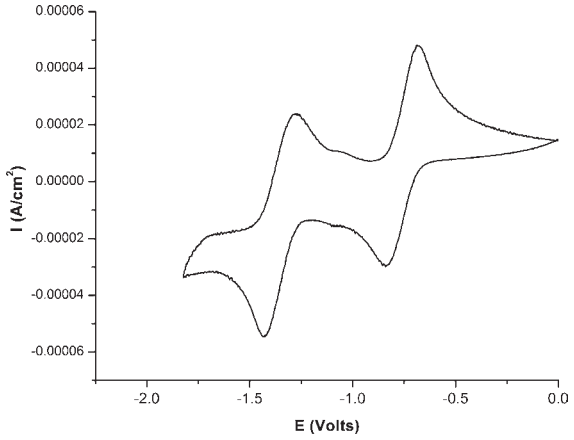

Figure 4. Cyclic voltammogram of **1** (10 mM) in DMF. Working electrode: glassy carbon disk. Counter electrode: platinum wire. Reference electrode: Ag/AgCl wire. Electrolyte: $[Bu_4N][PF_6]$, 100 mM. Scan rate: 200 mV/s.

centered reductions. Upon titration of the Ni(0)-species with $[(DME)NiBr_2]$ under conditions that generate and precipitate **1** in tetrahydrofuran (THF) solvent (red line, Figure 5), the growth of **1** can clearly be seen. On the time scale of the cyclic voltammogram studies, 1.5 equiv of $[(DME)NiBr_2]$ was used to push the reaction to completion.

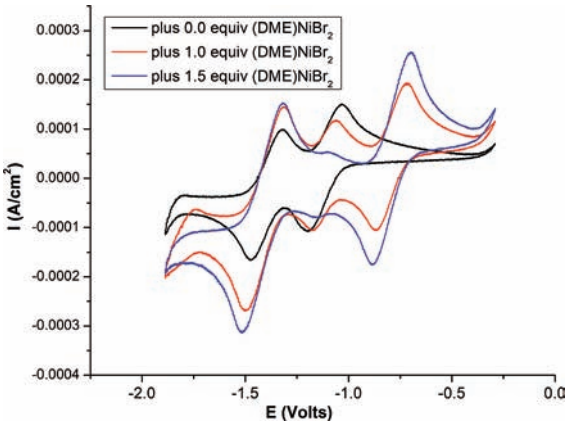

Figure 5. Cyclic voltammograms of DMF solutions of $[Ni(COD)_2]$ (20 mM) plus 2 equiv of terpyridine plus various equivalents of $[(DME)NiBr_2]$. Working electrode: glassy carbon disk. Counter electrode: platinum wire. Reference electrode: Ag/AgCl wire. Electrolyte: $[Bu_4N][PF_6]$, 200 mM. Scan rate: 200 mV/s.

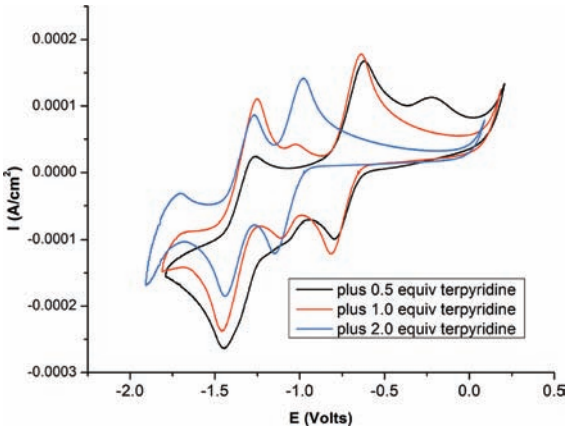

Figure 6. Cyclic voltammograms of DMF solutions of $[(DME)NiBr_2]$ (50 mM) plus various equivalents of terpyridine. Working electrode: glassy carbon. Counter electrode: platinum. Reference electrode: Ag/AgCl. Electrolyte: $[Bu_4N][PF_6]$, 400 mM. Scan rate: 200 mV/s.

A complementary experiment where titration of the nickel(II) source $[(DME)NiBr_2]$ with free terpyridine ligand was performed is shown in Figure 6. Addition of 1 equiv of terpyridine to generate $[(tpy)NiBr_2]$ leads to a wave (red line, Figure 6) that is indistinguishable to that seen growing in Figure 5. These studies suggest that the first two reductions of both **1** and $[(tpy)NiBr_2]$ are ligand-centered reductions and are to some extent independent of the oxidation state of the metal. DFT calculations show that the lowest unoccupied molecular orbitals (LUMOs) of **1** and $[(tpy)NiBr]^+$ are in fact qualitatively similar (see below). Addition of two full equivalents of terpyridine (Figure 6, blue line) to generate the known $[(tpy)_2Ni]Br_2$ provides the expected waves[12] at −1.07 and −1.36 V vs Ag/Ag^+. It is again noteworthy that the formally Ni(II) salt $[(tpy)_2Ni]Br_2$ displays a nearly identical cyclic voltammogram to the Ni(0) species resulting from the reaction of $Ni(COD)_2$ with 2 equiv of terpyridine (Figure 5 vs Figure 6). Thus, the overall ligand sphere (one vs two coordinated terpyridine

Table 1. Results of DFT Geometry Optimizations of 1 with Population Analyses

entry	basis set	starting geometry	energy (HF)	Mulliken spin density on Ni
1	6-31g**	bent	−4822.4884896	0.205394
2	6-31+g*	bent	−4822.2133401	1.128636
3	m6-31g* on Ni 6-31+g* on Br 6-31g* on C,H,N	bent	−4822.1102282	1.180345
4	m6-31g* on Ni 6-31+g* on Br 6-31g* on C,H,N	X-ray	−4822.1102234	1.180300
5	6-31g**	X-ray[a]	−4822.2745029	0.520126
6	m6-31g* on Ni 6-31+g* on Br 6-31g* on C,H,N	X-ray[a]	−4821.9117422	1.206290

[a] Single point energy calculations were performed without geometry optimizations.

ligands) plays more of a role in determining the redox potentials of these derivatives than do the formal oxidation states of the nickel ions in the solution phase.

Finally, DFT calculations were performed to lend support to the experimental evidence for a Ni(I) formulism for complex **1** in the solid state. Unrestricted geometry optimizations with no symmetry constraints, starting from both the bent form (angles modeled after the X-ray structure of [(tpy′)Ni-I]) and the X-ray coordinates, were performed along with population analyses, and selected results are shown in Table 1. As evident from Table 1, the calculated populations were somewhat sensitive to the basis sets employed, as the 6-31g** basis set consistently calculated a smaller metal contribution to the singly occupied molecular orbital (SOMO). The m6-31g* basis set,[13] which is optimized for first-row transition metals, calculated nearly the same spin density on nickel for both the geometry optimization and the single point SCF calculation (entries 4 and 6). All single point energy calculations based on the frozen geometry in the X-ray structure of **1** (entries 5 and 6) gave imaginary frequencies, whereas the full unrestricted geometry optimizations gave none. Interestingly, the bent [(tpy)Ni-Br] complexes all refine to near planar forms, while the bent [(tpy)Ni-I] retains its shape in a geometry optimization. A speculation is that the nonplanarity of the latter is a consequence of the large size of the iodide ligand.

Despite the differences in the population analyses, all geometry optimizations afforded roughly equivalent square planar structures (see Supporting Information) with significant amounts of electron density residing on the nickel atom. The calculated geometry (based on the method used in Table 1, entry 4) maintains the square-planar geometry in the gas-phase with a calculated *trans* N−Ni−Br angle of 179.998°. A plot of the SOMO of **1** from the same calculation is shown in Figure 7, and the $d_{x^2-y^2}$ component to the SOMO correlates well with the EPR data. The LUMO of **1** is also shown in Figure 7, along with that of its one-electron oxidized form. Population analyses were also run and compared to those previously calculated for [(tpy)Ni-CH_3] and [(tpy)Ni-I].[2] Chart 2 shows that for both [(tpy)Ni-I] and [(tpy)Ni-Br], the majority of the spin density resides on the metal. The calculated bond lengths (Chart 3) also do not show any major disruptions in the aromaticity of the ligand, consistent with a metal-centered radical.[14,15] Also of note is the longer nickel−nitrogen bond lengths of **1** compared with [(tpy)Ni-CH_3] (Chart 3), consisted with the antibonding nature of the $d_{x^2-y^2}$ in the SOMO of **1**. The location of the spin densities found for [(tpy)Ni-I] and [(tpy)Ni-Br] is in sharp contrast to that observed for [(tpy)Ni-CH_3], where over 90% of the spin density was calculated to reside on the ligand.[2]

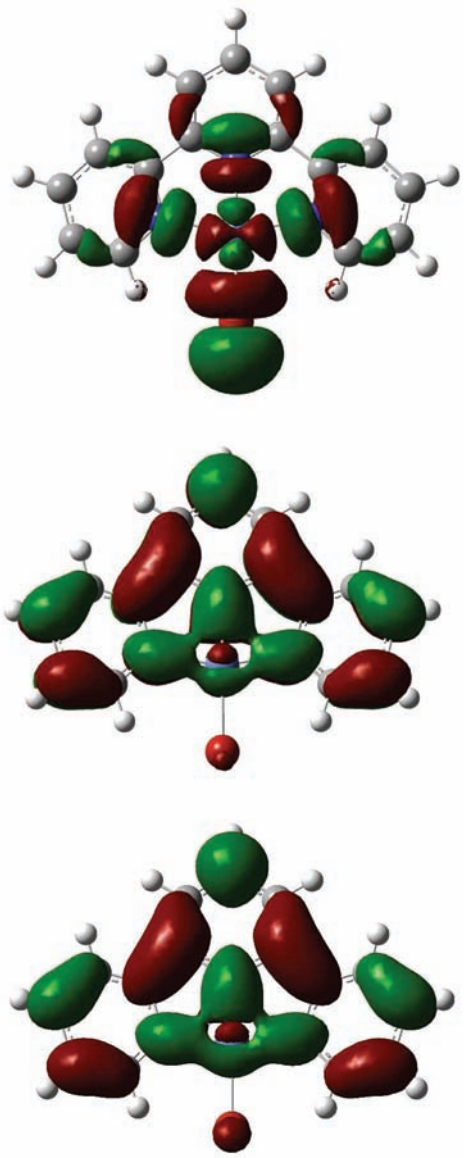

Figure 7. Top: SOMO of complex **1** from unrestricted DFT calculations (Table 1, entry 4). Selected bond lengths (Å): Ni−Br 2.389; Ni−N1 2.089; Ni−N2 1.933, Ni−N1a 2.089. Selected bond angles (deg): N2−Ni−Br 179.998; N2−Ni−N1 79.181, N1−Ni−Br 100.819, N1−Ni−N1a 158.363. Middle: Graphical representation of the LUMO of **1**. Bottom: Graphical representation of the LUMO of $[(tpy)Ni\text{-}Br]^+$ (singlet form).

CONCLUDING REMARKS

As more catalytic processes are being developed with the less costly and more abundant first-row metals, it is important to have a full understanding of the fundamental properties of the more

Chart 2. Calculated Spin Densities for Four-Coordinate Terpyridine Complexes[a]

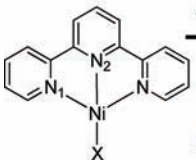

Population Analysis	[(tpy)Ni-CH$_3$]			[(tpy)Ni-Br]				[(tpy)Ni-I]		
	Ni	N2	N1	Ni	N2	N1	Br	Ni	N2	N1
Löwdin	0.087	0.179	0.059	1.171	-0.001	0.021	0.054	1.022	0.076	0.059
Mulliken	0.076	0.187	0.063	1.180	-0.003	0.014	0.067	1.034	0.076	0.063

[a]Calculations for [(tpy)Ni-Br] were based on Table 1, entry 4.

Chart 3. DFT-Calculated Bond Lengths for 1[a]

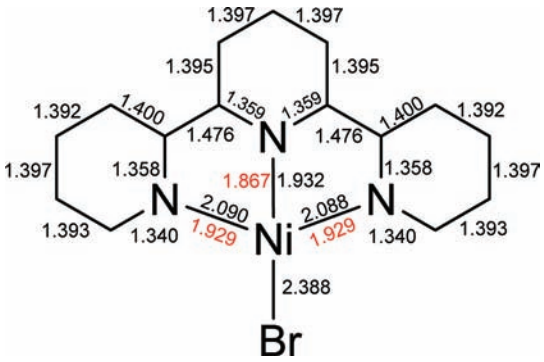

[a]Calculations for **1** were based on Table 1, entry 4. Bond lengths in red are those calculated for [(tpy)Ni-CH$_3$].[2]

active catalysts. Here, we have initiated studies on a catalytically active species present in a variety of nickel-mediated organic transformations and found that although the geometries of LNi-X and LNi-R may be quite similar, the electronic and magnetic properties can vary substantially. In particular, the replacement of an organometallic ligand like a methyl group with a simple halide can significantly alter the character of a SOMO in a molecule containing a redox active ligand. The much stronger σ bonding methyl ligand in [(tpy)Ni-CH$_3$] evidently raises the $d_{x^2-y^2}$ frontier orbital higher than does the bromide counterpart, making it preferable to put an electron in the terpyridine ligand.

EXPERIMENTAL PROCEDURES

General Considerations. All manipulations were performed using standard Schlenk and high vacuum techniques[16] or in a nitrogen filled glovebox. Solvents were degassed and passed over activated alumina columns before use. DMF was distilled over BaO under vacuum. A Rigaku SCXMini diffractometer was used for X-ray structure determinations. All EPR spectra were recorded on a Bruker EMXplus spectrometer. All cyclic voltammetry experiments were referenced to Ag/AgCl and calibrated to internally added decamethylferrocene ($E_{1/2}$ = 86 mV in DMF).[17]

Preparation of [(tpy)NiBr] (1). A yellow-orange solution of 0.1000 g of terpyridine (0.429 mmol) in 3 mL of THF was added to a stirring suspension of 0.0593 g of Ni(COD)$_2$ (0.216 mmol) in ~2 mL of THF. Within a few minutes, the solution had turned dark blue. After stirring at room temperature for 45 min, a purple solution of 0.0666 g of NiBr$_2$(dme) (0.216 mmol) in 5 mL of THF was added to the stirred blue solution. The resulting green suspension was stirred at room temperature for 8 h, and then cooled to −25 °C for approximately 40 h. The dark green solid was collected on a frit and dried under vacuum to yield 0.1149 g of [(tpy)NiBr]. Yield is 72.0%. Anal. Calcd (found) for $C_{15}H_{11}BrN_3Ni$: C, 48.45 (48.57); H, 2.98 (2.89). The paramagnetic NMR spectrum is provided in the Supporting Information.

Electronic Structure Calculations. Quantum calculations were performed with the Gaussian09W software.[18] Unconstrained geometry optimizations were performed using the B3LYP exchange-correlation functional.[19] Basis sets were used as described in the text. Note that the most consistent definition of the SOMO of a doublet state is the charge natural orbital whose occupation number is close to 1, and this was used in this work. The occupation number in the case of **1** was exactly 1. All calculations have been checked for the presence or absence of imaginary frequencies as described in the text.

ASSOCIATED CONTENT

Supporting Information. Crystallographic, DFT, and NMR data for **1**. This material is available free of charge via the Internet at http://pubs.acs.org.

AUTHOR INFORMATION

Corresponding Authors

*E-mail: yulia@iopc.ru (Y.H.B.), vicic@hawaii.edu (D.A.V.).

ACKNOWLEDGMENT

D.A.V. thanks the Office of Basic Energy Sciences of the U.S. Department of Energy (DE-FG02-07ER15885). The authors would also like to thank John Head for helpful discussions regarding the DFT calculations.

REFERENCES

(1) Anderson, T. J.; Jones, G. D.; Vicic, D. A. *J. Am. Chem. Soc.* **2004**, *126*, 8100.
(2) Jones, G. D.; Martin, J. L.; McFarland, C.; Allen, O. R.; Hall, R. E.; Haley, A. D.; Brandon, R. J.; Konovalova, T.; Desrochers, P. J.; Pulay, P.; Vicic, D. A. *J. Am. Chem. Soc.* **2006**, *128*, 13175.
(3) Jones, G. D.; McFarland, C.; Anderson, T. J.; Vicic, D. A. *Chem. Commun.* **2005**, 4211.
(4) Lin, X.; Phillips, D. L. *J. Org. Chem.* **2008**, *73*, 3680.
(5) Gong, H.; Gagne, M. R. *J. Am. Chem. Soc.* **2008**, *130*, 12177.
(6) Gong, H.; Sinisi, R.; Gagne, M. R. *J. Am. Chem. Soc.* **2007**, *129*, 1908.
(7) Gong, H.; Andrews, R. S.; Zuccarello, J. L.; Lee, S. J.; Gagne, M. R. *Org. Lett.* **2009**, *11*, 879.
(8) Mikhaylov, D. Y.; Budnikova, Y. H.; Gryaznova, T. V.; Krivolapov, D. V.; Litvinov, I. A.; Vicic, D. A.; Sinyashin, O. G. *J. Organomet. Chem.* **2009**, *694*, 3840.
(9) Mikhaylov, D. Y.; Budnikova, Y. H.; Gryaznova, T. V.; Dudkina, Y.; Khrizanphorov, M.; Kataeva, O.; Vicic, D. A. *Dalton Trans.* **2011**, submitted for publication.
(10) Prinsell, M. R.; Everson, D. A.; Weix, D. J. *Chem. Commun. (Cambridge, U.K.)* **2010**, *46*, 5743.

(11) Joshi-Pangu, A.; Ganesh, M.; Biscoe, M. R. *Org. Lett.* **2011**, *13*, 1218.
(12) Kuo, Y.-M. *J. Ch. Colloid Interface Soc.* **1992**, *15*, 23.
(13) Mitin, A. V.; Baker, J.; Pulay, P. *J. Chem. Phys.* **2003**, *118*, 7775.
(14) Ray, K.; Petrenko, T.; Wieghardt, K.; Neese, F. *Dalton Trans.* **2007**, 1552.
(15) Sproules, S.; Wieghardt, K. *Coord. Chem. Rev.* **2010**, *254*, 1358.
(16) Vicic, D. A.; Jones, G. D. In *Comprehensive Organometallic Chemistry III*; Crabtree, R. H., Mingos, D. M. P., Eds.; Elsevier: Amsterdam, The Netherlands, 2006; Vol. 1.
(17) Noviandri, I.; Brown, K. N.; Fleming, D. S.; Gulyas, P. T.; Lay, P. A.; Masters, A. F.; Phillips, L. *J. Phys. Chem. B* **1999**, *103*, 6713.
(18) Frisch, M. J. et al. *Gaussian 09*, Revision A.1; Gaussian, Inc.: Wallingford, CT, 2009. For the full reference, see Supporting Information.
(19) Becke, A. D. *J. Chem. Phys.* **1993**, *98*, 5648.